Chinese Chemical Letters 37 (2026) 111595

Contents lists available at ScienceDirect

Chinese Chemical Letters

journal homepage: www.elsevier.com/locate/cclet

Both promoting tetracycline decomposition in combination with CO_2 reduction for flower-like MoS_2 modified by Ti_3C_2 MXene quantum dots

Ziyu Yao[a,b], Huan Yang[a,b], Luyang Zuo[a,b], Fang Wang[a,b,*]

[a] Key Laboratory of Magnetic Molecules and Magnetic Information, Materials of Ministry of Education & School of Materials Science and Engineering of Shanxi Normal University, Taiyuan 030006, China
[b] Shanxi Key Laboratory of Advanced Magnetic Materials and Devices & Research Institute of Materials Science of Shanxi Normal University, Taiyuan 030006, China

ARTICLE INFO

Article history:
Received 30 May 2025
Revised 2 July 2025
Accepted 16 July 2025
Available online 16 July 2025

Keywords:
Piezo-photocatalytic technology
Dual-functional catalytic system
Decomposition of antibiotics
Stable CO_2 reduction
Ti_3C_2 MXene quantum dots

ABSTRACT

The utilization of piezo-photocatalytic technology to achieve the efficient decomposition of antibiotics and stable CO_2 reduction (dual-functional catalytic system) represents a cutting-edge approach for concurrently mitigating environmental pollution and the energy crisis. In this work, Ti_3C_2 MXene quantum dots with high electrical conductivity were uniformly modified on the surface of three-dimensional flower-like MoS_2, aiming to realize the piezo-photocatalytic degradation of tetracycline hydrochloride (TC-HCl) coupled with the reduction of CO_2 to CO. Remarkably, the degradation rate constant of the optimal Ti_3C_2 MXene quantum dots/MoS_2 sample reached 0.178 min^{-1}, which was 7.7 times higher than that of pure MoS_2 under single photocatalysis and 7.1 times higher than that under single piezocatalysis. Meanwhile, the CO yield rates reached 28 μmol g^{-1} h^{-1}, which was 4.6 times and 6.5 times higher than that of the single catalytic systems based on MoS_2, respectively. The introduction of Ti_3C_2 MXene quantum dots significantly enhanced the current density, charge transfer efficiency, and light absorption capacity, and also effectively suppressed the recombination of electron-hole pairs. This work provides a novel strategy for MoS_2-based composites to construct a dual-functional catalytic system *via* piezo-photocatalytic technology, offering a potential solution to address the concurrent challenges of environmental pollution and the energy crisis.

© 2026 Published by Elsevier B.V. on behalf of Chinese Chemical Society and Institute of Materia Medica, Chinese Academy of Medical Sciences.

In the current realm of environmental and energy research, the coexistence of diverse pollutants and energy-related challenges necessitates the development of innovative approaches [1]. Among these concerns, the contamination caused by antibiotics and the escalating atmospheric carbon dioxide (CO_2) levels stand out as two of the most critical issues [2]. Tetracycline hydrochloride (TC-HCl), as a common antibiotic, has been effectively utilized in treating bacterial infections in animals [2,3]. However, the abuse and incomplete metabolism of tetracycline have made it an emerging source of water pollution, posing a significant threat to animal health and ecological friendliness [4–7]. Simultaneously, the continuous increase in atmospheric CO_2 concentration, predominantly due to fossil fuel combustion, has triggered global warming and a cascade of associated environmental problems [8]. Converting CO_2 into valuable fuels is considered a promising strategy to mitigate both the energy crisis and the greenhouse effect [9]. However, conventional methods for antibiotic degradation and CO_2 reduction suffer from several limitations, including low catalytic efficiency, extended treatment durations, and high processing costs [8]. Therefore, the integrated process of efficiently degrading antibiotics while reducing CO_2 into fuel has emerged as a focal point of research, aiming to tackle both environmental pollution and the energy crisis.

At present, advanced oxidation processes (AOPs) including photocatalysis, piezocatalysis, piezo-photocatalysis, provide green and efficient solutions for decomposing antibiotics [4]. Photocatalysis can make full use of light energy to convert into chemical energy, forming electron and hole pairs on the catalyst surface [1]. The strong oxidation ability of holes is enough to directly decompose antibiotics, and the strong reducing property of electrons can reduce CO_2 to usable fuel [2]. Nevertheless, the development of highly efficient photocatalysts has been hampered by the rapid recombination of photogenerated electron-hole pairs and the constraints imposed by the light environment [3]. The piezo-photocatalytic technology that utilizes the piezoelectric effect of materials to promote photocatalytic reactions can compensate for the shortcomings of a single photocatalyst [10]. In a typical piezo-

* Corresponding author.
E-mail address: wangfanghc@sxnu.edu.cn (F. Wang).

https://doi.org/10.1016/j.cclet.2025.111595
1001-8417/© 2026 Published by Elsevier B.V. on behalf of Chinese Chemical Society and Institute of Materia Medica, Chinese Academy of Medical Sciences.

catalytic process, mechanical disturbances induce localized polarization charges in piezoelectric materials. These charges subsequently form an internal electric field, enabling the spatial separation of holes and free electrons [11]. Choosing photocatalytic materials with piezoelectric effect can achieve the conversion of mechanical/solar energy to chemical energy, which promotes more active substances participate in the degradation process of organic pollutants coupled with the CO_2 reduction process [10–12].

Recently, more and more researches have revealed that semiconductor photocatalytic materials also exhibit good piezoelectric catalytic ability (piezo-photocatalysis), such as one-dimensional (1D) ZnO nanorods [13], two-dimensional (2D) Bi_2WO_6 nanosheets [14] and three-dimensional (3D) flower-like MoS_2 [15]. Among them, 3D MoS_2 has a thin layer structure, unique piezoelectric properties, larger specific surface area, and more abundant active sites, making it a star candidate for the preparation of highly efficient catalysts for degrading antibiotics and CO_2 reduction [16–20].

While single piezo-photocatalysts can address the issue of light-dependence and enhance the separation efficiency of charge carriers, their catalytic activity still has significant room for improvement [21–23]. Anchoring metal and quantum dots particles on the surface of semiconductor catalysts can further reduce the probability of carrier recombination and increase active sites, making it an effective method for constructing efficient catalysts [21–28]. Consequently, the surface modification strategy holds great potential for enabling composite piezo-photocatalysts to achieve remarkable performance in the simultaneous degradation of antibiotics and reduction of CO_2.

As a rising star co-catalyst, 2D Ti_3C_2 MXene can promote the separation and migration of photoinduced electron-hole pairs after coupled with MoS_2 [29–33]. Zero-dimensional (0D) Ti_3C_2 MXene quantum dots extracted from two-dimensional Ti_3C_2 MXene flakes exhibit better dispersibility, larger bandgap (quantum confinement effect), negative Fermi level, and richer active edge sites compared to the matrix material [34–36]. Various Ti_3C_2 MXene QDs modification composite such as Ti_3C_2 quantum dots/Cu_2O nanowire/Cu [30], Ti_3C_2 quantum dots/g-C_3N_4 nanosheets [37], and Ti_3C_2 quantum dots/BiOBr [38] have been synthesized, and it has been verified that Ti_3C_2 quantum dots can enhance charge transfer efficiency, charge density, and stability, thereby significantly improving photocatalytic degradation, hydrogen production, and CO_2 reduction ability [30,37]. Therefore, Ti_3C_2 MXene QDs modified on the surface of 3D MoS_2 is a feasible method to build ultra-high activity catalysts, which is induced by visible light irradiation and ultrasound vibration.

Herein, we successfully synthesized the novel Ti_3C_2 MXene quantum dots/MoS_2 (TDM) piezo-photocatalysts by hydrothermal reaction. The modification of an appropriate amount of Ti_3C_2 MXene quantum dots on the surface of MoS_2 significantly enhances the efficiency of piezo-photocatalytic degradation of antibiotics coupled with CO_2 reduction. It is worth noting that Ti_3C_2 MXene quantum dots with good conductivity are introduced into 3D flower-like MoS_2, resulting in a significant increase in photocurrent density and a significant decrease in electrochemical impedance. Moreover, the mechanical strain produced by ultrasonic activation directly provides a built-in piezoelectric field, which facilitates the accelerated transfer of photo-excited carriers at the interface from MoS_2 to Ti_3C_2 MXene quantum dots. Furthermore, the possible mechanism of dual-functional catalytic system of piezo-photocatalytic system is also expounded.

Synthesis process diagram of Ti_3C_2 MXene quantum dots/MoS_2 composites is shown in Fig. 1. The XRD patterns of TDM0 (pure MoS_2), TDM1, TDM2, TDM3 and TDM4 are presented in Fig. 2a. The main diffraction peaks of TDM0 are indexed to pure MoS_2 with lattice constants $\alpha = 3.16$ and $c = 12.294$ Å (JSPDS No. 37-1492), respectively [4]. The crystal structure of primordial Ti_3AlC_2 and Ti_3C_2 are shown in Fig. S1 (Supporting information). The FESEM image depicted in Fig. 2b clearly demonstrates the morphology of pure 3D flower-like MoS_2. The particles have sizes smaller than 500 nm and are composed of irregular nanoplates, endowing them with a substantial number of active surface areas [15]. After the combination of Ti_3C_2 MXene quantum dots and MoS_2, the appearance of TDM2 composite does not exhibit significant alterations (Fig. 2c). The morphology of accordion-like Ti_3C_2 MXene and HRTEM image of Ti_3C_2 MXene quantum dots are displayed in Fig. S2 (Supporting information), providing insights into their structural characteristics. Fig. 2d reveals the HRTEM image of TMD2 specimen. It is evident that the lattice fringes with interplanar space of 0.62 nm and 0.26 nm are corresponding to the (002) plane of MoS_2 and (0110) plane of Ti_3C_2 MXene quantum dots [15,35]. Significantly, a large number of ultrathin lamellar MoS_2 stretches into flat surface, which is beneficial to expose more active sites for catalytic reaction. Other SEM images of TDM1, TDM3 and TDM4 are exhibited in Fig. S3 (Supporting information), offering a comprehensive view of the morphological characteristics of these samples. TEM images of TDM0 and TDM2 samples are presented in Fig. S4 (Supporting information). Figs. 2e and f present the STEM and EDS mapping images to explore the distribution of elements in TDM2 sample. The colorful mapping images vividly illustrate the distribution of Ti, C, Mo, and S elements.

Piezoelectric force microscope (PFM) is one of the convictive method to research the functional properties of piezoelectric materials in nanoscale [39]. It can be obtained that the surface heights of TDM2 (Fig. 3a) fluctuate in the range of -172∼148 nm and in a randomly selected 2×2 μm^2 surface area. Upon applying a +5 V voltage to the surface of the as-prepared composites, the relative amplitude images (Fig. 3b) and phase switching signals (Fig. 3c) reveal that piezoelectric response is generated in TDM2. Particularly, the piezoelectric potential of TDM2 fluctuates in the range of -1.6∼1.4 V, suggests that TDM2 specimen possesses moderate piezoelectricity.

The chemical composition and elemental states of TDM0 and TDM2 were investigated using X-ray photoelectron spectroscopy (XPS). As shown in Fig. 3d, the presence of Mo, S, Ti, and C elements was detected, which is in good agreement with the results of EDS mappings. Characteristic peaks at 36.5, 160.9, 227, 283.8, and 529.7 eV can be assigned to Ti 3p, S 2p, Mo 3d, C 1s, and O 1s, respectively [33]. Fig. 3e gives the high resolution Mo 3d spectra of the composites. The binding energies of Mo $3d_{5/2}$ and Mo $3d_{3/2}$ peaks in MoS_2 are located at 226.71 and 229.92 eV, revealing the existence of Mo^{3+} in TDM [18]. The Mo 3d peaks of TDM2 shift to 226.43 and 229.57 eV, respectively, indicating that the strong interaction is emerged between MoS_2 and MXene quantum dots. The S 2p spectra of TDM0 and TDM2 are displayed in Fig. 3f. The two peaks in TDM2 sample situated at 159.38 and 160.61 eV can be ascribed to S $2p_{3/2}$ and S $2p_{1/2}$, respectively, which is slightly lower than pure MoS_2 (159.64 and 160.8 eV) [22]. Fig. S5 depicts the N_2 adsorption-desorption isotherms of TDM0 and TDM2. The typical IV isotherm illustrates the mesoporous properties of the composites [28].

The transfer and recombination of photogenerated charges were investigated by PL spectroscopy (Fig. 3g). The absorption peak intensity of TDM2 samples was significantly lower than TDM0, indicating that charge and hole recombination ability are effectively inhibited. The separation efficiency of photo-generated holes and electrons is characterized by the transient photocurrent response (*I-t* curves, measured under light with ultrasonic vibration), as shown in Fig. 3h. TDM2 exhibited higher photocurrent intensity than TDM0, which is ascribed to the rapid migration of electrons from the conduction band of MoS_2 to Ti_3C_2 MXene quantum dots [35]. For comparison, the photocurrent density images of TDM0 and TDM2 without ultrasonic vibration are shown in Fig. S6 (Sup-

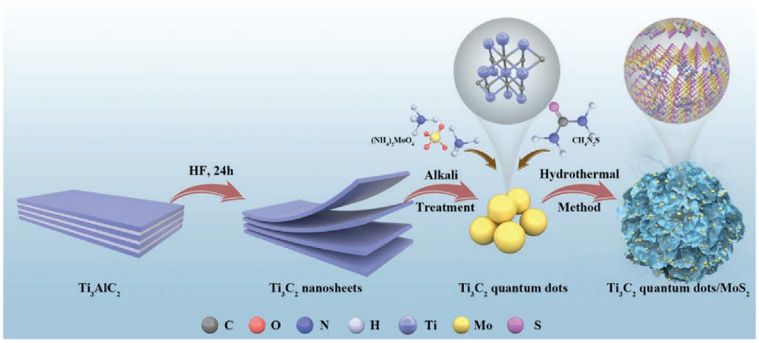


Fig. 1. Synthesis process diagram of Ti_3C_2 MXene quantum dots/MoS_2 composites.

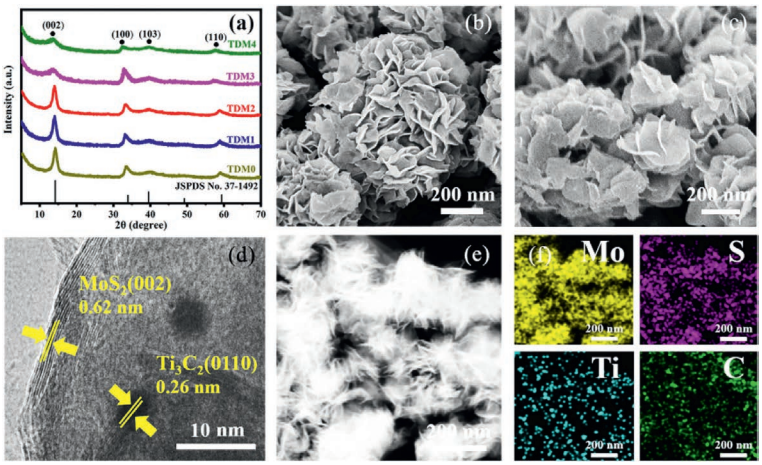


Fig. 2. (a) XRD patterns of TDM composites. FESEM images of (b) TDM0 and (c) TDM2 samples. (d) HRTEM image and (e, f) element mappings of TDM2 specimen.

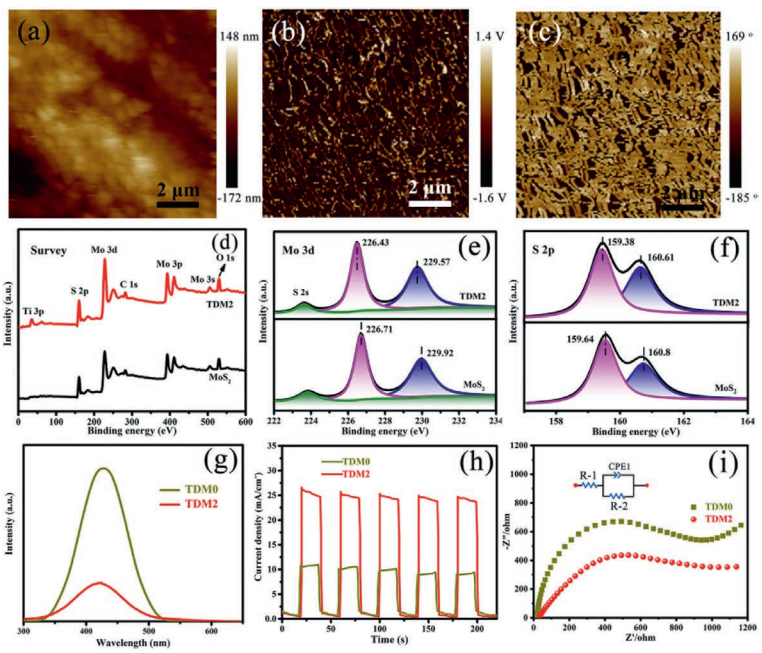


Fig. 3. (a) AFM morphology, (b) PFM amplitude, and (c) phase image of TDM2. (d) XPS survey spectra and high resolution XPS spectra of (e) Mo 3d, (f) S 2p of TDM0 and TDM2. (g) Stead-state photoluminescence (PL) spectra, (h) transient photocurrent response (with ultrasonic vibration), and (i) electrochemical impendence spectra (with ultrasonic vibration) of as-prepared samples.

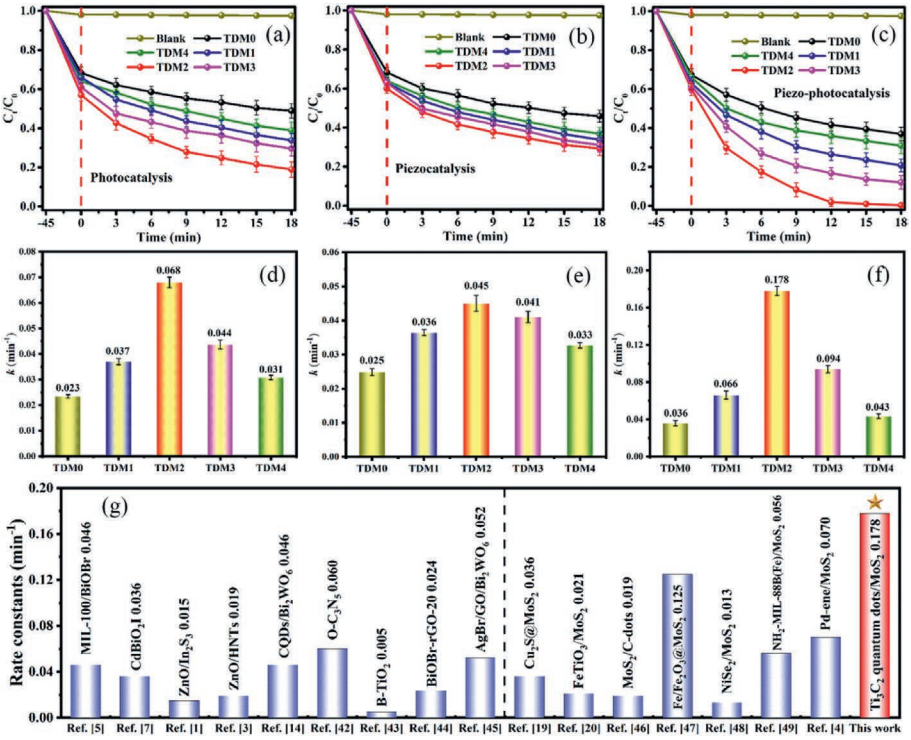


Fig. 4. Degradation curves and corresponding reaction rate constant of TDM0 (MoS2), TDM1, TDM2, TDM3, and TDM4 samples (TC-HCl, 20 mg/L) under different conditions of (a, d) photocatalysis, (b, e) piezocatalysis, and (c, f) piezo-photocatalysis. (g) Comparison of TC-HCl degradation rate constants in the reported reference.

porting information). This result indicates that ultrasonic vibration can effectively increase the transfer rate of photo-generated carriers. The charge recombination/transfer behavior (Fig. 3i) of TDM0 and TDM2 is confirmed by electrochemical impendence spectra (with ultrasonic vibration). The arc radius of TDM2 was smaller than TDM0, which implies a fast interfacial charge-transfer process and more effective separation of photo-induced carriers [36]. The UV-vis diffused reflectance spectra (DRS) of TDM0 and TDM2 are shown in Fig. S7 (Supporting information).

Fig. 4 presents the decomposition curves and reaction rate constants of TC-HCl (20 mg/L) degradation under different condition (visible light, ultrasonic activation, both visible light and ultrasonic vibration), which reveals the piezocatalytic process, photocatalytic reaction and piezo-photocatalysis of composites. All adsorption effects are eliminated before degradation experiments by stirring the mixtures in the dark for 45 min. The chemical stability of TC-HCl molecules is confirmed by the blank experiment in all degradation situations.

As depicted in Figs. 4a and d, the photocatalytic performance was evaluated by removal of TC-HCl under visible light irradiation. Obviously, the synthesized TDM composites have stronger photocatalytic performance than MoS_2. Specifically, TDM2 demonstrated a higher degradation activity with a reaction rate constant of 0.068 min^{-1}, surpassing that of TDM0 (0.023 min^{-1}). Under the same experimental conditions, the degradation ratios of TC-HCl for TDM1, TDM3, and TDM4 were approximately 67 %, 71 %, and 61 %, respectively. The corresponding values of reaction rate were 0.037, 0.044, and 0.031 min^{-1}. The piezocatalytic performance (Figs. 4b and e) of as-prepared samples is assessed by the degradation of TC-HCl under ultrasonic vibration in the dark. The TDM2 sample demonstrates an optimal piezocatalytic degradation efficiency, achieving 72 % degradation of TC-HCl within 18 min. The raised catalytic activity illustrates that piezoelectric effect generated by vibrating MoS_2 is enhanced in the heterostructures [10].

The piezo-phototronic effect realizes the piezoelectric conversion and photoelectric conversion, which plays the essential role in the piezo-photocatalytic system [23]. The piezo-photocatalytic activity was appraised under the combined action of visible light irradiation and ultrasonic vibration for the decomposition of TC-HCl in aqueous solution (Figs. 4c and f). The enhanced catalytic ability of TDM samples in piezo-photocatalytic system reflects the piezo-phototronic effect remarkably improve the catalytic performance of as-prepared composites. It is gratifying that TC-HCl molecules were completely degradation with a rate of 0.178 min^{-1} over TDM2, far better than TDM0, TDM1, TDM3, and TDM4. This result indicates that the local surface piezoelectric field initiated by ultrasonic vibration in TDM2 accelerates the separation and migration of photoinduced carriers in the TC-HCl degradation process, resulting in more piezo-photoelectrons participating in the piezo-photocatalytic reaction [39]. Compared with the TDM2 sample, the lower catalytic performance of the TDM1 sample is due to the lower loading of Ti_3C_2 MXene quantum dots, which limits the migration of photogenerated electrons to quantum dots. The low catalytic performance of TDM3 samples is attributed to the high loading of Ti_3C_2 MXene quantum dots, which hinders the light absorption of MoS_2 and covers the catalytic active sites [14,27]. The temporal UV-vis absorption spectral (Fig. S8 in Supporting information) reflects the entire piezo-photocatalytic process of TC-HCl decomposition in the presence of TDM2 powders.

The main oxidative species in the catalytic degradation reaction were detected by free radicals trapping experiments [40], as given in Fig. S9 (Supporting information). The stability property of TDM2 was assessed by repeating 5 times in the piezo-photocatalytic tests (Fig. S10 in Supporting information). After 5 cycles of piezo-photocatalysis, the catalytic activity decreased by less than 10 %. This result further confirms that the built-in piezoelectric field induced by ultrasound can sustain the separation of photogenerated carriers and facilitate the migration of electrons [41].

Fig. 4g provides a comprehensive summary of recent research findings regarding the reaction rate constants of tetracycline hydrochloride under various catalytic systems [1,3–5,7,14,19,20,42–49]. More detailed catalytic decomposition information is summa-

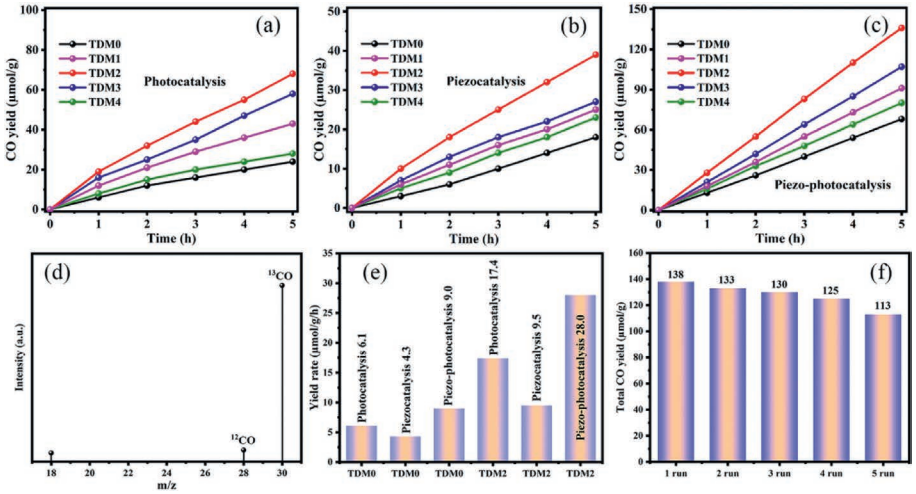


Fig. 5. CO yield of (a) photocatalysis, (b) piezocatalysis, and (c) piezo-photocatalysis of as-prepared samples. (d) The isotope-labelled $^{13}CO_2$ experiment. (e) Photoredox activity of TDM0 and TDM2 under various reaction conditions. (f) The piezo-photocatalytic CO yields after 5 h reaction in 5 consequtive runs of TDM2.

rized in Table S1 (Supporting information). The structural stability of TDM2 is exhibited by comparing the XRD and SEM before and after use [50], as shown in Figs. S11 and S12 (Supporting information). The comparison shows that after 5 cycles of tests, the structure of the TDM composite material did not change significantly. The decrease in catalytic performance may be caused by the adsorption of pollutants. Through these comparisons, any potential structural changes can be accurately identified, providing valuable insights into the durability and reliability of the TDM2 catalyst in practical applications.

The TDM composites not only demonstrate extremely high catalytic performance in the degradation of tetracycline, but also show better performance during the simultaneous reduction of CO_2 to CO [9]. Figs. 5a-c show the amount of CO generated by TDM in different catalytic scenarios (photocatalysis, piezocatalysis, and piezo-photocatalysis), respectively. Among these, the TDM2 sample consistently showcased the most outstanding catalytic activity. Within a period of 5 h, the CO yields for TDM2 reached 68.2, 39.6, and 136.4 μmol/g under photocatalysis, piezocatalysis, and piezo-photocatalysis, respectively.

Since the decomposition of tetracycline also produces a small amount of CO and CO_2, the $^{13}CO_2$ labeling experiment (Fig. 5d) was used to detect the source of CO_2. Once $^{13}CO_2$ in the system was employed as the reaction gas, ^{13}CO ($m/z = 29$) can be observed. If the CO_2 produced by the decomposition of tetracycline was utilized as the reaction gas, ^{12}CO ($m/z = 28$) were obtained [2]. It can be observed from the figure that both ^{13}CO ($m/z = 29$) and a small amount of ^{12}CO ($m/z = 28$) were present. This observation strongly indicates that both the initially introduced CO_2 and the CO_2 generated during the degradation of tetracycline participated in the overall reaction.

The CO yield rates of TDM0 and TDM2 samples in different reaction systems (photocatalysis, piezocatalysis, and piezo-photocatalysis) are shown in Fig. 5e. The CO yield rates of TDM0 in photocatalysis, piezocatalysis and piezo-photocatalysis systems are 6.1, 4.3 and 9 μmol g^{-1} h^{-1}, while the CO yield rates of TDM2 are 17.4, 9.5 and 28 μmol g^{-1} h^{-1}, respectively. The optimal TDM2 sample is 4.6 and 6.5 times that of TDM0 in single photocatalysis and piezocatalysis, respectively. The cycling stability of the TDM2 sample was verified by 5 times consecutive CO_2 reduction experiments (Fig. 5f) [51]. The output of CO decreased from 138 μmol/g to 113 μmol/g, indicating that the sample has strong cycling stability. The observed reduction in CO production can likely be attributed to the adsorption of organic pollutants during the cyclic process, as well as potential losses incurred during the cleaning and drying steps [52].

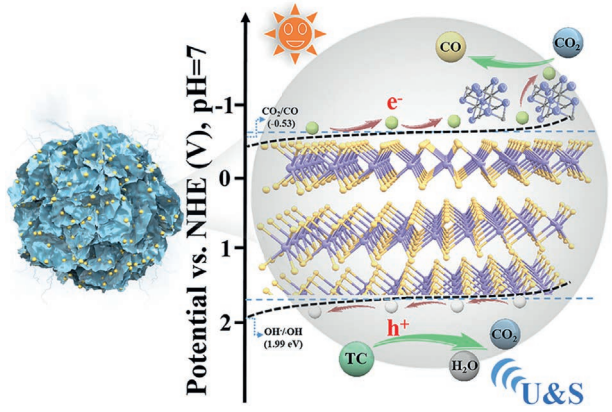


Fig. 6. Schematic illustration of the charge migration mechanism of TDM2 composite in the piezo-photocatalytic reaction.

The crystallographic representations of MoS_2 are displayed in Fig. S13 (Supporting information). It can be observed from the side view crystallography that each unit cell is asymmetrically composed by two S atoms on the left and one Mo atom on the right. The MoS_2 reveals single layer of Mo between two S layers with identical bonding length of Mo-S ≈ 2.418 Å to form a hexagonal structure (top view). The side view further illustrates the free strain characteristics of the Mo-2S dipoles, along with the tensile and compressive strains that occur when pressure is applied. When the Mo-S dipole is subjected to tensile stress, a spontaneous polarization occurs, with the polarization site shifting from the S atom to the Mo atom along the direction of the bond. Consequently, the built-in piezoelectric field propagates in the opposite direction. Conversely, when the Mo-S dipole experiences compression, the polarization point moves from the Mo atom to the S atom, leading to the generation of an opposite built-in electric field [41]. The electric field created by the external force (F_0) acts as a crucial driving force, effectively facilitating the separation of photogenerated electrons and holes in opposite directions.

The possible mechanism underlying the piezo-photocatalytic TC-HCl decomposition coupled with CO_2 reduction of CO in Ti_3C_2 MXene quantum dots/MoS_2 heterojunction is illustrated in Fig. 6. Without energy intervention, TC-HCl molecules, CO_2, and catalysts

are randomly distributed in the solution and do not interact with each other. Subsequently, light energy and mechanical energy are introduced into the system. Under the excitation of light energy, MoS_2 semiconductor generates photoelectric charges and holes in the conduction band (CB) and valence band (VB) (Fig. S14 in Supporting information). Opposite positive and negative charges are generated on the opposite sides of the MoS_2 (piezoelectric effect), diffusing along a specific crystal direction [41]. When MoS_2 is subjected to ultrasonic vibration, it generates polarized charges and forms a piezoelectric electric field within or on the surface of the material. The accumulation of polarized positive (negative) charges at both ends of the MoS_2 molecule forces the energy band to bend in the direction of high (low) potential energy. Under the influence of the negative charge on the MoS_2 side, the CB of MoS_2 bends upward (at a low potential), and the strongly reducing electrons rapidly transfer to the surface of the Ti_3C_2 MXene quantum dots along the direction of the upward bend of the CB. These electrons on the surface of the MXene quantum dots then react with CO_2 molecules, facilitating the reduction of CO_2 to CO [9]. Simultaneously, the accumulation of positive charges on the other side of the MoS_2 forces the valence band in this region to shift downwards, towards a region of higher electrical potential. The holes located in the valence band move along the curved VB, directly oxidizing TC-HCl molecules or reacting with H_2O to generate hydroxyl radicals ($^{\bullet}OH$). Finally, the holes and electrons generated by the absorption of light energy move and are consumed in opposite directions along the CB and VB. This effectively reduces the likelihood of recombination between holes and electrons, significantly enhancing the efficiency of the coupled process of TC-HCl decomposition and CO_2 reduction in the piezo-photocatalytic reaction [53]. Under the action of positive and negative charges (provided by a piezoelectric field), electrons move towards the region of lower potential, while h^+ moves in the opposite direction towards a high potential, forming a closed loop in space. As a result, the electron-hole pairs are rapidly separated through the piezo-phototronic effect of the piezo-photocatalytic system, which is endowed by the combination of the photocatalytic heterojunction and the piezoelectric field.

In summary, Ti_3C_2 MXene quantum dot/MoS_2 (TDM) piezo-photocatalyst were successfully synthesized *via* a one-step hydrothermal method. Compared with the single-function catalysis reported in the previous literature, TDM catalysts are capable of achieving efficient decomposition of tetracycline hydrochloride while simultaneously enabling stable reduction of CO_2 to CO. Compared with the single catalytic system of pure MoS_2, the catalytic degradation rate and CO yield of TDM2 samples reach 0.178 min^{-1} and 28 μmol g^{-1} h^{-1} respectively, which are more than 7 times and 4 times higher. The uniformly distributed Ti_3C_2 MXene quantum dots with high conductivity not only enhance the light absorption, photocurrent and specific surface area of the composite, but also reduce the electrochemical impedance. The built-in electric field provided by ultrasonic oscillation serves as an effective driving force to separate photogenerated carriers. Electrons and holes move in opposite directions relative to the external force, forming a closed circuit in conjunction with the piezoelectric field. This work indicates that the surface modification strategies of MoS_2 that incorporate piezoelectric photoelectronic effects hold significant promise for their application in the efficient antibiotic degradation coupled CO_2 reduction.

CRediT authorship contribution statement

Ziyu Yao: Writing – review & editing, Writing – original draft, Methodology, Conceptualization. **Huan Yang:** Methodology. **Luyang Zuo:** Formal analysis, Conceptualization. **Fang Wang:** Resources, Funding acquisition.

Declaration of competing interest

The authors declare that they have no known competing financial interests or personal relationships that could have appeared to influence the work reported in this paper.

Acknowledgment

This work is supported by the National Natural Science Foundation of China (Nos. U24A2023, 52371191, 52301244).

Supplementary materials

Supplementary material associated with this article can be found, in the online version, at doi:10.1016/j.cclet.2025.111595.

References

[1] Y. Ai, J. Hu, X. Xiong, et al., Appl. Catal. B: Environ. Energy 353 (2024) 124098.
[2] X. Li, J. Cao, X. Jia, et al., Appl. Catal. B: Environ. Energy 362 (2025) 124713.
[3] L. Zhang, J. Cheng, Y. Shi, et al., Chin. Chem. Lett. 35 (2024) 110400.
[4] C. Liu, J. Li, C. Guo, et al., Chem. Eng. J. 502 (2024) 157909.
[5] B. Xue, C. Yang, P. Guo, et al., Appl. Surf. Sci. 30 (2025) 162552.
[6] X. Hua, H. Chen, C. Rong, et al., J. Hazard. Mater. 448 (2023) 130951.
[7] W. Zheng, Z. Zhu, R. Sha, et al., J. Materiomics 11 (2025) 100928.
[8] L. Lu, H. Zhang, Z. Sun, et al., Chem. Eng. J. 477 (2023) 146892.
[9] X. Jia, H. Sun, H. Lin, et al., Appl. Surf. Sci. 614 (2023) 156017.
[10] C. Xi, R. Tan, Q. Ai, et al., Nano Energy 132 (2024) 110415.
[11] D. Gautam, L. Saya, G. Gambhir, et al., Chem. Eng. J. 498 (2024) 154987.
[12] Y. Cheng, T. Yu, X. Lei, et al., Chem. Eng. J. 504 (2025) 158900.
[13] X. Zhou, Y. Liu, Y. Miao, et al., Sep. Purif. Technol. 323 (2023) 124410.
[14] H. Ren, F. Qi, A. Labidi, et al., Appl. Catal. B: Environ. 330 (2023) 122587.
[15] T. Yu, H. Guo, J. Yu, et al., J. Alloy. Compd. 997 (2024) 174938.
[16] Y. Li, Z. Lai, Z. Huang, et al., Appl. Surf. Sci. 550 (2021) 149342.
[17] S. Sun, Q. An, M. Watanabe, et al., Appl. Catal. B: Environ. 271 (2020) 118931.
[18] G. Qin, X. Song, Q. Chen, et al., Appl. Catal. B: Environ. Energy 344 (2024) 123640.
[19] A. Negi, A. Chauhan, Kirti, et al., J. Clean. Prod. 450 (2024) 141829.
[20] P. Zhu, Y. Li, F. Chen, et al., J. Alloy. Compd. 937 (2023) 168425.
[21] B. Shen, Y. Chen, L. Zhao, et al., J. Colloid Interface Sci. 684 (2025) 226–243.
[22] Y. Wang, Y. Lin, F. Zha, et al., J. Colloid Interface Sci. 652 (2023) 936–944.
[23] H. Li, Y. Sang, S. Chang, et al., Nano Lett. 15 (2015) 2372–2379.
[24] Y. Li, Q. Wang, H. Wang, et al., J. Colloid Interface Sci. 537 (2019) 206–214.
[25] C. Chen, C. Ye, X. Zhao, et al., Nat. Commun. 15 (2024) 7825.
[26] J. Di, J. Xia, M. Ji, et al., ACS Sustain. Chem. Eng. 4 (2016) 136–146.
[27] Z. Yao, H. Sun, Y. Hu, et al., J. Materiomics 7 (2021) 1122–1130.
[28] Z. Yao, L. Zuo, H. Yang, et al., J. Colloid Interface Sci. 697 (2025) 137939.
[29] J. Peng, P. Ye, F. Xu, et al., Compos. Part B: Eng. 284 (2024) 111731.
[30] Z. Zeng, Y. Yan, J. Chen, et al., Adv. Funct. Mater. 29 (2018) 1806500.
[31] P. Sun, Z. Xing, Z. Li, et al., Chem. Eng. J. 458 (2023) 141399.
[32] L. Zhao, P. Zhang, L. Li, et al., Chemosphere 361 (2024) 142547.
[33] J. Yang, Q. Zhu, Z. Xie, et al., J. Alloy. Compd. 887 (2021) 161411.
[34] Q. Xue, H. Zhang, M. Zhu, et al., Adv. Mater. 29 (2017) 1604847.
[35] A. Wang, Y. Wen, H. Zhu, et al., Chem. Eng. J. 496 (2024) 154264.
[36] Q. Li, X. Cui, X. Liu, et al., J. Alloy. Compd. 1011 (2025) 178399.
[37] B. Chang, Y. Guo, H. Liu, et al., J. Mater. Chem. A 10 (2022) 3134–3145.
[38] T. Cheng, Z. Xing, N. Zhang, et al., Chemosphere 364 (2024) 143255.
[39] Z. Yao, H. Sun, S. Xiao, et al., Appl. Surf. Sci. 560 (2020) 150037.
[40] L. Lu, N. Liang, H. Sun, et al., J. Materiomics 8 (2022) 47–58.
[41] J. Wu, W. Chang, Y. Chang, et al., Adv. Mater. 28 (2016) 3718–3725.
[42] T. Wang, N. Song, S. Yao, et al., Chem. Eng. J. 495 (2024) 153379.
[43] S. Wu, H. Hu, Y. Lin, et al., Chem. Eng. J. 382 (2020) 122842.
[44] M. Shkir, S.H. Aldirham, S. AlFaify, et al., Chemosphere 357 (2024) 141934.
[45] Z. Guan, X. Li, Y. Wu, et al., Chem. Eng. J. 410 (2021) 128283.
[46] S. Zhang, Z. Xu, T. Ji, et al., Sep. Purif. Technol. 353 (2025) 128148.
[47] G. Li, B. Gu, Y. Luo, et al., J. Environ. Manage. 353 (2024) 120210.
[48] J. Jia, L. Zheng, K. Li, et al., Chem. Eng. J. 429 (2022) 132432.
[49] X. Feng, R. Long, C. Liu, et al., Sep. Purif. Technol. 302 (2022) 122138.
[50] H. Yang, F. Wang, H. Zhang, et al., J. Am. Chem. Soc. 142 (2020) 4438–4444.
[51] D. Liu, B. Sun, S. Bai, et al., Chin. J. Catal. 50 (2023) 273–283.
[52] J. Tang, R. Guo, W. Zhou, et al., Appl. Catal. B: Environ. 237 (2018) 802–810.
[53] H. Li, B. Sun, T. Gao, et al., Chin. J. Catal. 43 (2022) 461–471.